ACS APPLIED MATERIALS & INTERFACES

Research Article

www.acsami.org

Manipulating Dispersion and Distribution of Graphene in PLA through Novel Interface Engineering for Improved Conductive Properties

Yu Fu,[†] Linshu Liu,[‡] and Jinwen Zhang*[,†]

[†]School of Mechanical and Materials Engineering, Composite Materials and Engineering Center, Washington State University, Pullman, Washington 99164, United States

[‡]Eastern Regional Research Center, Agricultural Research Service, U.S. Department of Agriculture, 600 East Mermaid Lane, Wyndmoor, Pennsylvania 19038, United States

Supporting Information

ABSTRACT: This study aimed to enhance the conductive properties of PLA nanocomposite by controlling the dispersion and distribution of graphene within the minor phase of the polymer blend. Functionalized graphene (*f*-GO) was achieved by reacting graphene oxide (GO) with various silanes under the aid of an ionic liquid. Ethylene/*n*-butyl acrylate/glycidyl methacrylate terpolymer elastomer (EBA-GMA) was introduced as the minor phase to tailor the interface of matrix/graphene through reactive compatibilization. GO particles were predominantly dispersed in PLA in a self-agglomerating pattern, while *f*-GO was preferentially located in the introduced rubber phase or at the PLA/EBA-GMA interfaces through the formation of the three-dimensional percolated structures, especially for these functionalized graphene with reactive groups. The selective localization of the *f*-GO also played a crucial role in stabilizing and improving the phase morphology of the PLA blend through reducing the interfacial tension between two phases. The establishment of the percolated network structures in the ternary system was responsible for the improved AC conductivity and better dielectric properties of the resulting nanocomposites.

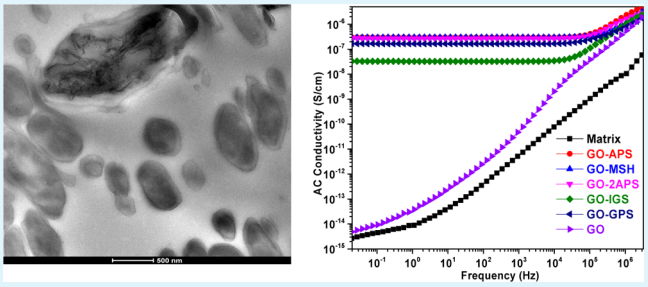

KEYWORDS: *graphene, functionalization, dispersion, polylactic acid, nanocomposites, conductivity*

INTRODUCTION

In recent years, environmentally friendly polylactic acid (PLA) nanocomposites have attracted a lot of attention. Introduction of a certain level of nanofillers improves the heat resistance of PLA materials. However, mechanical, thermal, and electrical properties of most reported PLA nanocomposites are still unsatisfactory for practical applications. Fine dispersion of nanofillers in the PLA matrix is still the key challenge due to its very high surface area to volume ratio. Surface treatment of the nanofillers is necessary to improve the dispersion of nanofillers in the polymer matrix and interfacial adhesion and is still the focus of manocomposite preparation.[1,2]

Because of its superior thermal and electrical properties, graphene has been added to various polymers to impart polymer nanocomposite improved electric, thermal, and mechanical properties.[3−10] Meanwhile, surface treatment of graphene has also been explored to manipulate the properties of polymer/graphene nanocomposites. For example, reduction of the isocyanate-functionalized graphene oxide in a solution with PS by dimethylhydrazine yielded conductive nanocomposites with an onset of electrical percolation at 0.1 vol %.[3] However, this advanced level of dispersion of graphene in polymers was realized by solution mixing of graphene and polymer. In the melt process, it is much more challenging to achieve a high level of dispersion of the nanosized fillers in polymer. Additionally, the aggregation of graphene in molten polymers can also play a substantially negative role in its dispersibility. For example, when the functionalized graphene was directly mixed with PMMA at a relatively high loading level (3 wt %), agglomeration was still noted in the system.[10]

Some reports in the literature have demonstrated that addition of conductive carbon nanofillers to polymer blends may simultaneously improve mechanical properties and electrical conductivity of the resulting nanocomposites through double percolation mechanism.[11−21] When a nanofiller is added to a polymer blend, it may preferably reside in one phase over the other due to its different affinity with two components. With the nanofiller-dispersed phase transformed from discrete domains into continuity in the system microscopically, the percolation threshold of nanofillers in the polymer matrix can be reduced to a much lower loading level. The success of this approach relies on selective localization of nanofillers and fine

Received: May 30, 2014
Accepted: July 4, 2014
Published: July 4, 2014

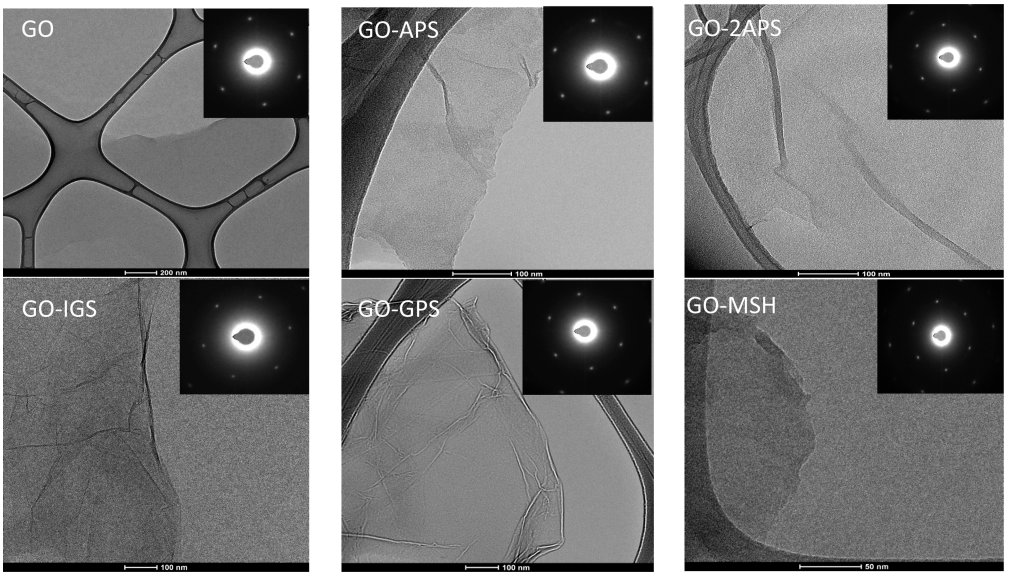

Figure 1. High-resolution TEM images of the *f*-GO with the corresponding selected area electron diffraction (SAED).

dispersion of nanofillers in the polymer blend. Practically, the nanofiller may selectively reside in either the individual phase or at the interface when both phases are cocontinuous. This approach not only results in a high level of electrical conductivity at relatively low loading of nanofillers but also avoids high processing viscosity associated with high nanofiller loading. Recently, many studies have found that the nanofillers, such as organoclay, can also act as interfacial modifiers in immiscible blend systems.[22−27] It is proposed that addition of nanofillers may influence the phase morphology by reducing the interfacial tension between two phases and finally resulting in a well-dispersed morphology. To play the role of interfacial modifier, the nanofillers need to be compatible with the two immiscible components or be mainly dispersed in the minor component and have better compatibility with the polymer host.

In our previous study of PLA toughening with an epoxy-containing elastomer toughener, that is, ethylene/*n*-butyl acrylate/glycidyl methacrylate copolymer (EBA-GMA), zinc-containing ionomer was used to both cross-link the elastomer and catalyze the interfacial compatibilization between EBA-GMA and PLA matrix.[28,29] If graphene is functionalized with some epoxy curing groups or some active groups, it may play a role of substitution for the ionomer and serve as a cross-linker for EBA-GMA in the above system. In such a new system, the functionalized graphene would selectively reside in the elastomer phase and/or at the interface. As a result, PLA composites of good conductive properties can probably be obtained at relatively low graphene loading levels.

With this rationale in mind, in this study, a novel ternary PLA composite system consisting of PLA, EBA-GMA, and functionalized graphene was introduced, and the electric properties of the resulting composites containing different functional graphenes were studied. The objective of this work is to investigate the effectiveness of graphene functionalization and the effects of elastomer modifier on graphene dispersion and other properties of the PLA/graphene composites. To the best of our knowledge, no similar studies have been reported in the literature.

EXPERIMENTAL SECTION

Materials. *Sample Preparation.* The preparations of functionalized graphene (*f*-GO) and PLA/*f*-GO nanocomposites can be found in our previous study.[30] Briefly, graphene was first functionalized by silane through a novel two-step method under the aid of an ionic liquid. Five silane agents (Supporting Information Scheme S1), 3-aminopropyl triethoxysilane (APS, 99%), 3-isocyanatopropyl triethoxysilane (IGS, 95%), 3-glycidyloxypropyl trimethoxysilane (GPS, 98%), 3-(2-aminoethylamino) propyl trimethoxylsilane (2APS, 97%), and 3-mercaptopropyl trimethoxysilane (MSH, 95%) were employed in the treatment, respectively. A masterbatch of 30 wt % *f*-GO in PLA was then prepared by mixing in the solution and then evaporating the solvent. The resulting masterbatch was compounded with PLA and EBA-GMA using a twin-screw microextruder (HAAKE Rheomex CTW5 minilab II) at 180 °C and a screw speed of ∼150 rpm for 5 min. For all samples, the PLA/EBA-GMA weight ratio was fixed at 80/20 because the formulation used with this weight ratio had exhibited the toughening effects on the PLA and been thoroughly studied in our previous papers.[28,29] The sheet samples of the nanocomposites were prepared using a Carver hot press (model 3912) and were used for further measurements. The resulting nanocomposites were designated as GO-*xn*, in which "*x*" and "*n*" refer to the different organofunctional groups and the content of the corresponding graphene, respectively.

Characterizations. The detailed characterization of *f*-GO including FT-IR, NMR, Raman, XRD, DSC, and TGA can be found in our early work. In this work, dispersibility and surface properties of *f*-GO were further evaluated using UV−vis, TEM, AFM, and XPS, respectively. Selective localization of *f*-GO in the composite matrix and the engineered interface were observed using a HRTEM. In addition, the electrical properties and wettability of the *f*-GO nanocomposites were studied using AC conductivity, dielectric testing, and contact angle measurement.

Morphology and Surface Analysis of f-GO. The morphology of the blend matrix and the *f*-GO nanocomposites was investigated using transmission electron microscopy (TEM, JEOL 1200EX) at an accelerated voltage of 100 kV. Ultrathin sections were cryogenically sliced using a RMC CR-X microtome equipped with a diamond knife and placed on Formvar coated 200-mesh nickel grids.

Atomic Force Microscopy (AFM). The aqueous suspension of *f*-GO was spin coated on freshly cleaved mica surfaces for AFM study. The solution was completely dried by evaporation at the ambient condition prior to testing. The AFM tests were conducted in tapping mode using a Veeco Multimode AFM equipped with a NanoScope IIIa controller (Digital Instruments Inc.). Sample surfaces were scanned in the air

using Si tips (Digital Instruments Inc.) with a resonance frequency of ca. 330 kHz at a scan rate of 0.4 Hz.

X-ray Photoelectron Spectroscopy (XPS). XPS spectra of the prepared samples were obtained with an AXIS-165 manufactured by Kratos Analytical Inc. (Spring Valley, NY) using achromatic X-ray radiation of 1253.6 eV (Mg Kα). Pass energy of 40 eV and spot size of about 120 μm were used to acquire all of the spectra. The spectrometer was calibrated against both the Au 4f7/2 peak at 84.0 eV and the Ag 3d5/2 peak at 368.3 eV.

UV–Visible Spectroscopy (UV–Vis). The UV–vis spectrum of the stable aqueous suspensions *f*-GO was recorded on a Nicolet Evolution 300 UV–visible spectrophotometer (Thermo Fisher Scientic Inc., U.S.) using a quartz cell in the wavelength range of 200–800 nm.

Conductivity and Dielectric Properties Measurement. A Novocontrol Technologies dielectric impedance analyzer (model Alpha-N) was used to measure the electrical conductivity of the compression molded nanocomposites (20 mm in diameter). A root-mean-square (rms) voltage of 1 V was applied over a frequency range of 10^{-2}–10^{6} Hz. To obtain reliable accuracy, each nanocomposite sample was repeated at least five times.

Wetting Behavior of the f-GO Nanocomposites. Static contact angles under air were measured by using an OCA 15 plus contact angle meter with a PC controlled motorized syringe. The average value of five measurements at different positions of the sheet surfaces was taken as the contact angle.

RESULTS AND DISCUSSION

Morphology and Surface Analysis of *f*-GO. The TEM images in Figure 1 implied that the single graphene sheet of *f*-GO was more inclined to scroll and wrinkle than that of GO. These evident ripples in the former were probably due to the large amount of silane chains grafted on the graphene sheet.[31] Their SAED patterns exhibited perfect hexagonal lattice and confirmed single layer graphene sheet characteristics of GO and *f*-GO (Figure 1, inset). Supporting Information Figure S1 shows the AFM images of the GO, GO-APS, and GO-MSH. The thickness of a single layer of GO was 1.0–1.3 nm and close to the typical value for one-atom-thick GO.[32,33] However, the thicknesses of single layer for the silane treated GO-APS and GO-MSH were in the range of 1.5–2 nm. The slight increase in thickness was attributed to the contribution of silane moieties heavily attached on the graphene surfaces.

Supporting Information Figure S2 shows the XPS spectra of GO and *f*-GO, and Table 1 gives the summary of the atomic

Table 1. XPS Analysis Results of Surface Composition of GO and *f*-GO

	relative atomic percentage of elements (%)					
sample	O	C	Si	N	S	O/C
GO	30.8	69.2				0.45
GO-APS	15.98	76.83	3.67	3.51		0.21
GO-2APS	11.54	80.7	2.33	5.43		0.14
GO-GPS	23.06	75.18	1.75			0.31
GO-IGS	23.23	73.28	1.39	2.11		0.32
GO-MSH	20.46	61.59	10.32		7.63	0.33

percentages of the samples. The results clearly indicated that silane treatment resulted in a great reduction of the oxygen-containing polar groups. Particularly, the increase of the C/O ratio suggested the graphene-like hydrophobic characteristic for the resulting *f*-GO. The relative content of Si in the *f*-GO varied greatly with the silane used. GO-MSH and GO-IGS gave the highest and lowest Si contents, respectively, while no Si was found in GO. Because all of the silane treatments were performed under the same conditions, the differences in the efficiency of functionalization were probably due to the difference in solubility for the silanes with different organo-functional groups. This decrease of the O/C ratio after treatment also suggested that the GO was simultaneously reduced during the functionalization due to deoxygenation of some oxygen-containing groups and restoration of the delocalized π-conjugated structure in the graphene from complete and effective exfoliation and stabilization of graphene sheets with the aid of the ionic liquid during the functionalization.

Figure 2 shows the UV–vis spectra of aqueous *f*-GO solutions. The maximum absorption at 233 nm and the broad

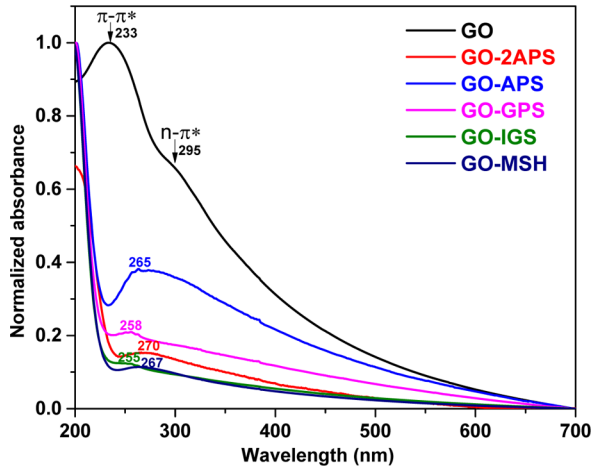

Figure 2. UV–vis spectra of stable aqueous suspensions of *f*-GO.

shoulder around 295 nm corresponded to the π–π* transition of the aromatic C–C bonds and the n–π* transitions of the C=O bonds, respectively. Silane functionalization caused a clear bathochromic red-shift to the GO peak at 233 nm, which appeared at 255–272 nm for *f*-GO. The disappearance of the C=O absorption peak and the slight difference of the original C–C peak shift in the *f*-GO suggested the π-conjugated network in the graphene sheets was partially restored. The difference in intensity of absorption for different *f*-GO was also observed. The GO aqueous solution offered the highest absorption intensity and therefore displayed the best dispersing ability in water, followed closely by GO-APS. GO-GPS, GO-2APS, GO-IGS, and GO-MSH exhibited very similar dispersibility in water. It is known that graphene is hydrophobic and GO is hydrophilic in nature. Therefore, different surface characteristics of GO and *f*-GO finally resulted in different dispersibility in water and other organic solvents.

Morphology of *f*-GO Composites. Some studies showed that nanofillers could stabilize the immiscible and partially miscible polymer blends and improved phase mophology.[34–36] Moreover, the stabilization could be affected by factors such as the interfacial energy between the polymers, the inhibition of coalescence by the presence of the rigid fillers around the dispersed polymer, and the viscosity difference between the two polymers caused by the filler–polymer interaction.[37] Apparently, the nanofiller selective localization in the polymer blend is a key factor to understand the observed compatibilization mechanism.

Figure 3 shows the TEM micrographs of the ternary PLA nanocomposites with different *f*-GO. In the neat PLA/EBA-

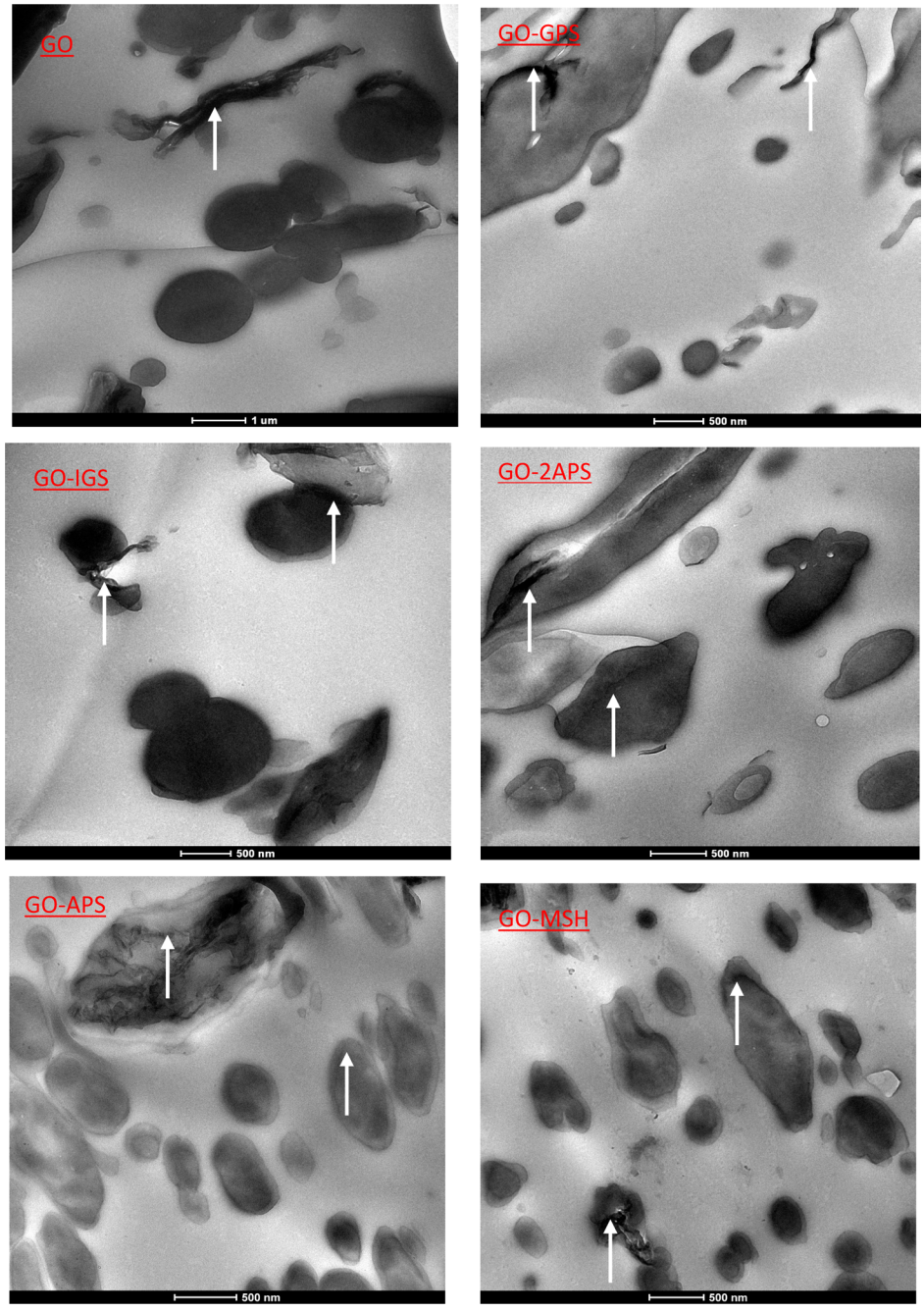

Figure 3. TEM micrographs of the ternary PLA nanocomposites with 5 wt % *f*-GO. White arrows indicate the location of *f*-GO in the blend matrix.

GMA blend, the rubber phase was well dispersed and homogeneously distributed as small droplets in the PLA matrix (micrograph not shown), suggesting better compatibilization between the two polymers as shown in our previous studies.[28,29] When GO was added to the blend, it was mainly distributed in the PLA phase. This result was in agreement with the theoretical prediction based on estimation of interfacial wetting between polymers and between polymer and GO or *f*-GO (details can be found in the Supporting Information). Furthermore, GO also exhibited some large agglomerates in the matrix because the interactions were mainly physical ones. However, when *f*-GO was added to the blends, they exhibited a preference to reside in the rubber phase and/or at the PLA/rubber interface. This result was contradictory to the theoretical estimation based on interfacial wetting, which also predicted the preferable residence of *f*-GO in PLA. This inconsistency in *f*-GO dispersion was because the determination of wetting parameter[38] did not take the interfacial chemical reactions between *f*-GO and EBA-GMA and/or PLA into account, however, which was the determining factor in compatibilizing the ternary composites. Cross-linking reaction between the epoxy groups of EBA-GMA and the amino groups of GO-APS and the mercapto groups of GO-MSH occurred during blending, respectively; therefore *f*-GO was predominantly retained in the rubber phase and/or at the rubber/PLA interface. On the contrary, the theoretical prediction is basically based on the physical interactions between the nanofillers and the polymers. Alternatively, the consistency in GO distribution between the TEM image and prediction based on wetting parameters indirectly confirmed that there is no or insignificant

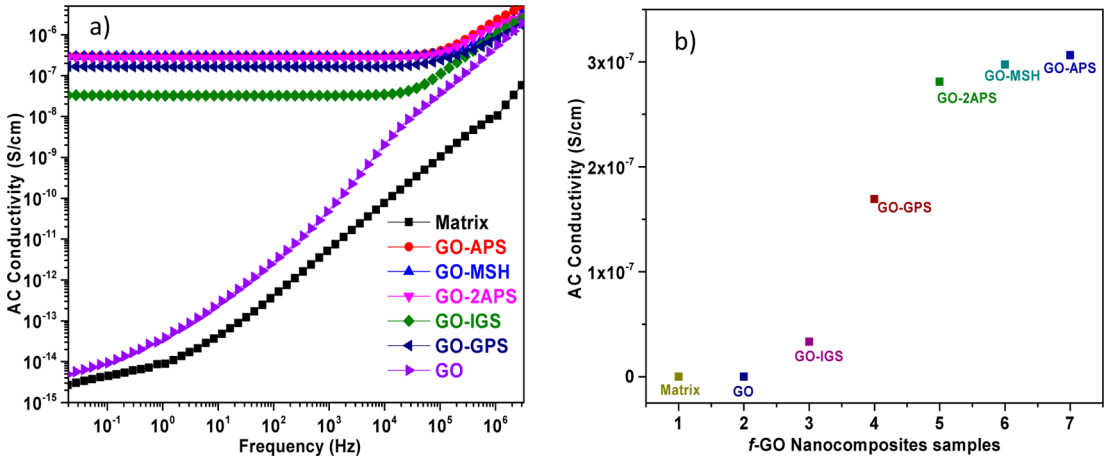

Figure 4. AC conductivity of the PLA ternary nanocomposites with 5 wt % *f*-GO: (a) AC conductivity versus frequency ranging from 10^{-2} to 10^{6} Hz; and (b) AC conductivity at 10^{-2} Hz.

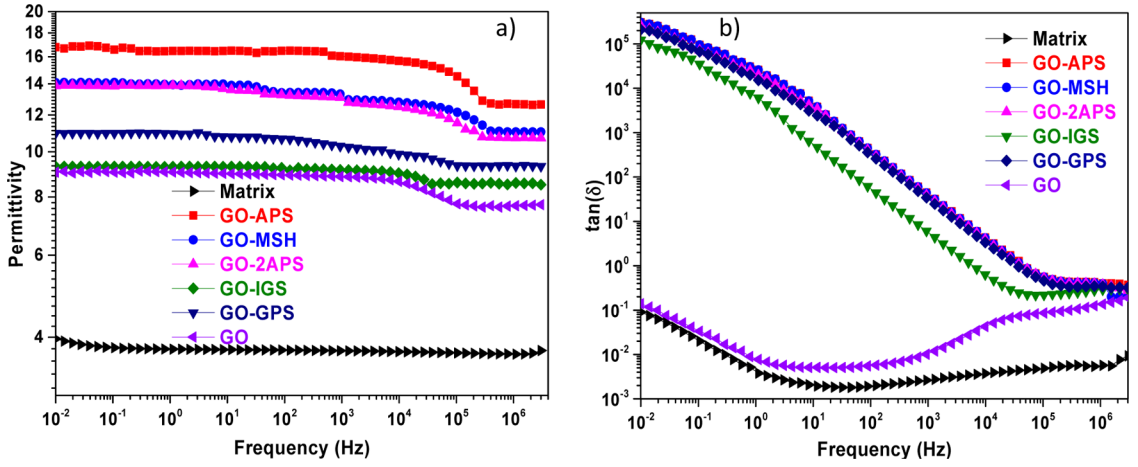

Figure 5. Dielectric properties of the PLA ternary nanocomposites with 5 wt % *f*-GO at frequency ranging from 10^{-2} to 10^{6} Hz.

chemical reactions between GO and polymers but significant chemical interactions between *f*-GO and polymers. In Figure 3, the rubber domains appeared irregular in the *f*-GO nanocomposites. Particularly, GO-APS, GO-2APS, and GO-MSH formed the fluffy network-like microstructures in the rubber phase. This selective location and distribution of *f*-GO in the composite matrix not only overcome the self-agglomeration of GO in PLA, but also stabilize the phase morphology of the blend by reducing the interfacial tension. On the other hand, selective distribution of GO and *f*-GO (GO-IGS and GO-GPS) with less reactive groups facilitated the occurrence of thermodynamically and kinetically driven compatibilization with the PLA except the chemical interactions. Furthermore, different wetting properties of GO and *f*-GO nanocomposites also indicated that surface characteristics of the resulting nanocomposites were changed significantly except the morphology (Supporting Information Figure S3). These results suggest that fine-tuning of graphene surface characteristics and the introduction of a second phase significantly improved the interfacial polymer structure and phase morphology and hence finally promoted interfacial compatibilization between graphene and PLA blend matrix.

AC Conductivity. Electrical conductivity of the nanocomposites is determined by the concentration of conductive nanofillers in the matrix phase and structure continuity of the resulting nancomposites. Therefore, the distribution of different conductive nanofillers in the polymer blend and their interface characteristics can be estimated by the electrical conductivity of the resulting nanocomposites.[39] Figure 4 shows the AC conductivities with frequency ranging from 10^{-2} to 10^{6} Hz at room temperature for the blend matrix and nanocomposites. The PLA blend and the nanocomposite with 5 wt % GO exhibited the typical frequency-dependent AC conductivity, which increased almost linearly with the increase of frequency. However, the nanocomposites with 5% *f*-GO exhibited AC conductivities, which were almost independent of the change of frequency in the low frequency range. This result indicated that effective three-dimensional conductive networks were formed in these *f*-GO nanocomposites and the AC conductivity became independent of frequency. The observed difference in percolation threshold between the GO and *f*-GO suggests that they had different interfacial compatibility with the matrix and existed in different dispersion state and distribution in the PLA due to the addition of the second minor rubber phase. Especially, for these *f*-GO with amino- and mercapto-functional groups and above the percolation threshold, the occurring of cross-linking reaction with EBA-GMA during blending further intensified the resulting effective 3-D conductive networks. Therefore, the introduction of the rubber phase enabled selective localization of *f*-GO and improved

exfoliation and dispersion of *f*-GO in the PLA and finally resulted in the improved interfacial adhesion and distribution with the fine dispersion and uniform distribution of rubber phase in the PLA.

As reported by other researchers, AC conductivity at low frequency is equal to or very close to DC conductivity.[40] Figure 4b shows the comparison of the AC conductivity of the blend and its *f*-GO nanocomposites at a very low frequency (10^{-2} Hz). An obvious increase in AC conductivity was noted from the matrix to the *f*-GO in the order of matrix, GO, GO-IGS, GO-GPS, GO-2APS, GO-MSH, and GO-APS. Thus, it can reasonably be assumed that the formation of cross-linking network structures facilitated the electron transport through electron hopping along graphene interconnects.[41,42]

Dielectric Properties. Permittivity of a material represents the ability to store a charge when the material is subjected to an electric field and reflect the dielectric properties of the material. Figure 5a shows the permittivity and dielectric loss of the *f*-GO nanocomposites with frequency ranging from 10^{-2} to 10^{6} Hz at room temperature. The PLA blend and all *f*-GO nanocomposites exhibited permittivities that were similarly frequency-independent but varied greatly in magnitude. Some studies have shown that the improvement of the dielectric properties is from the Maxwell–Wagner–Sillars (MWS) polarization for heterogeneous systems, associated with the free charges entrapped in the interfaces.[42] Therefore, the difference in permittivity possibly originated from the different characteristics of the molecular order and the thickness of the interphase. The GO nanocomposite exhibited lower permittivity than the *f*-GO nanocomposites, which was due to the formation of large agglomerates and the poor interfacial adhesion between the GO and the EBA-GMA and PLA because only physical blending existed in the system. Such agglomerates also decreased the total interface area and made less free charges retained or entrapped in the interfaces. In the other *f*-GO nanocomposites, the increased dielectric properties suggested that these nanofillers were well dispersed, surrounded by the PLA through the bridge of rubber phase, and finally generated the increased interfacial area from the enlarged thickness of the interphase and strong interfacial adhesion. As a result, more free charges were entrapped in their interphases.

It is well-known that the dielectric loss is a measurement of energy dissipation from the movement or rotation of the molecules in the external electric field. Therefore, the magnitude of dielectric loss can be used to evaluate the interfacial adhesion between the nanofillers and the matrix in the nanocomposites. Figure 5b shows the changes of dielectric loss among the matrix and *f*-GO nanocomposites with frequency ranging from 10^{-2} to 10^{6} Hz at room temperature. For the GO nanocomposite, the dielectric loss exhibited a weak frequency dependence in the whole frequency range because of the poor interfacial compatibility or weak interfacial interactions between the GO and the blend matrix. Although the second minor phase was introduced, reactive compounding occurred for GO. Thus, less molecules or dipoles could move or rotate, and less energy was dissipated. However, for other *f*-GO nanocomposites, more interfacial areas were created due to the cross-linking reaction between the *f*-GO and composite matrix and the improved interfacial interactions with the composite matrix, and polymer chains were separated into smaller domains by the conductive network formed so that the movement of molecules or rotation of dipoles could become more active and energetic. Thus, more energy could be dissipated so that higher dielectric loss was observed. This was consistent with the TEM analysis of these nanocomposites.

CONCLUSIONS

The novel design of composite matrix was developed to enable selective localization of *f*-GO and facilitate the interfacial modifications to tailor specific interfacial polymer structure and properties. By manipulating the dispersion and distribution of graphene with a minor polymer phase, the interfacial structure and properties of graphene and PLA can be tuned for property improvement. It was confirmed that with the help of well-dispersed EBA-GMA in PLA, some *f*-GO may homogeneously reside in the minor phase through the reactive compounding and finally be uniformly distributed in the PLA matrix, thereby improving graphene/matrix interfacial adhesion. Unlike the GO agglomerations in the PLA phase, the functionalized graphene was well dispersed and homogeneously distributed in the composite matrix through reactive compatibilization with the PLA and formed the continuous conductive network structures, producing higher AC conductivity and better dielectric properties. The structure continuity of the matrix phase and the formation of a 3-D effective conductive network were verified by the improved electrical conductivity and dielectric properties of the *f*-GO nanocomposites. These findings may contribute to the future development of high-performance multifunctional graphene nanocomposites.

ASSOCIATED CONTENT

Supporting Information

Chemical structure of silane used, AFM morphology of GO-APS and GO-MSH, deconvolution of the C 1s peak of the XPS spectra of GO and *f*-GO, theoretical prediction of the location of the *f*-GO in the blend matrix, and static contact angles of water and diiodomethane on the *f*-GO nanocomposite sheet surfaces. This material is available free of charge via the Internet at http://pubs.acs.org.

AUTHOR INFORMATION

Corresponding Author

*Tel.: (509) 335-8723. Fax: (509) 335-5077. E-mail: jwzhang@wsu.edu.

Notes

The authors declare no competing financial interest.

REFERENCES

(1) Ganguli, S.; Roy, K.; Anderson, P. Improved Thermal Conductivity for Chemically Functionalized Exfoliated Graphite/Epoxy Composites. *Carbon* **2008**, *46*, 806–817.

(2) Monica Veca, L. Polymer Functionalization and Solubilization of Carbon Nanosheets. *Chem. Commun.* **2009**, *18*, 2565–2567.

(3) Stankovich, S.; Dikin, A.; Dommett, H.; Kohlhaas, M.; Zimney, J.; Stach, A.; Piner, D.; Nguyen, T.; Ruoff, S. Graphene-based Composite Materials. *Nature* **2006**, *442*, 282–286.

(4) Cerezo, F.; Preston, C.; Shanks, R. Structural, Mechanical and Dielectric Properties of Poly (ethylene-co-methyl acrylate-co-acrylic acid) Graphite Oxide Nanocomposites. *Compos. Sci. Technol.* **2007**, *67*, 79–91.

(5) Liang, J.; Huang, Y.; Zhang, L.; Wang, Y.; Ma, Y.; Guo, T.; Chen, Y. Molecular-Level Dispersion of Graphene into Poly (vinyl alcohol) and Effective Reinforcement of their Nanocomposites. *Adv. Funct. Mater.* **2009**, *19*, 2297–2302.

(6) Salavagione, H. J.; Martínez, G.; Gómez, M. A. Synthesis of Poly (vinyl alcohol)/Reduced Graphite Oxide Nanocomposites with

Improved Thermal and Electrical Properties. *J. Mater. Chem.* **2009**, *19*, 5027−5032.
(7) Yang, X.; Li, L.; Shang, S.; Tao, X.-M. Synthesis and Characterization of Layer-aligned Poly (vinyl alcohol)/Graphene Nanocomposites. *Polymer* **2010**, *51*, 3431−3435.
(8) Cai, D.; Song, M. A Simple Route to Enhance the Interface between Graphite Oxide Nanoplatelets and a Semi-crystalline Polymer for Stress Transfer. *Nanotechnology* **2009**, *20*, 315708.
(9) Ansari, S.; Kelarakis, A.; Estevez, L.; Giannelis, E. P. Oriented Arrays of Graphene in a Polymer Matrix by In-situ Reduction of Graphite Oxide Nanosheets. *Small* **2010**, *6*, 205−209.
(10) Goncalves, G.; Marques, P.; Barros-Timmons, A.; Bdkin, I.; Singh, M. K.; Emami, N.; Gracio, J. Graphene Oxide Modified with PMMA via ATRP as a Reinforcement Filler. *J. Mater. Chem.* **2010**, *20*, 9927−9934.
(11) Foulger, S. H. Reduced Percolation Thresholds of Immiscible Conductive Blends. *J. Polym. Sci., Part B: Polym. Phys.* **1999**, *37*, 1899−1910.
(12) Göldel, A.; Kasaliwal, G.; Pötschke, P. Selective Localization and Migration of Multiwalled Carbon Nanotubes in Blends of Polycarbonate and Poly (styrene-acrylonitrile). *Macromol. Rapid Commun.* **2009**, *30*, 423−429.
(13) Gubbels, F.; Jérôme, R.; Teyssie, P.; Vanlathem, E.; Deltour, R.; Calderone, A.; Parente, V.; Brédas, J.-L. Selective Localization of Carbon Black in Immiscible Polymer Blends: a Useful Tool to Design Electrical Conductive Composites. *Macromolecules* **1994**, *27*, 1972−1974.
(14) Levon, K.; Margolina, A.; Patashinsky, A. Z. Multiple Percolation in Conducting Polymer Blends. *Macromolecules* **1993**, *26*, 4061−4063.
(15) Li, Y.; Shimizu, H. Conductive PVDF/PA6/CNTs Nanocomposites Fabricated by Dual Formation of Cocontinuous and Nanodispersion Structures. *Macromolecules* **2008**, *41*, 5339−5344.
(16) Mallette, J.; Marquez, A.; Manero, O.; Castro-Rodríguez, R. Carbon Black Filled PET/PMMA Blends: Electrical and Morphological Studies. *Polym. Eng. Sci.* **2000**, *40*, 2272−2278.
(17) Sumita, M.; Sakata, K.; Asai, S.; Miyasaka, K.; Nakagawa, H. Dispersion of Fillers and the Electrical Conductivity of Polymer Blends Filled with Carbon Black. *Polym. Bull.* **1991**, *25*, 265−271.
(18) Sumita, M.; Sakata, K.; Hayakawa, Y.; Asai, S.; Miyasaka, K.; Tanemura, M. Double Percolation Effect on the Electrical Conductivity of Conductive Particles Filled Polymer Blends. *Colloid Polym. Sci.* **1992**, *270*, 134−139.
(19) Wu, D.; Zhang, Y.; Zhang, M.; Yu, W. Selective Localization of Multiwalled Carbon Nanotubes in Poly (ε-caprolactone)/Polylactide Blend. *Biomacromolecules* **2009**, *10*, 417−424.
(20) Wu, G.; Miura, T.; Asai, S.; Sumita, M. Carbon Black-Loading Induced Phase Fluctuations in PVDF/PMMA Miscible Blends: Dynamic Percolation Measurements. *Polymer* **2001**, *42*, 3271−3279.
(21) Zhang, M. Q.; Yu, G.; Zeng, H. M.; Zhang, H. B.; Hou, Y. H. Two-step Percolation in Polymer Blends Filled with Carbon Black. *Macromolecules* **1998**, *31*, 6724−6726.
(22) Khatua, B. B.; Lee, D. J.; Kim, H. Y.; Kim, J. K. Effect of Organoclay Platelets on Morphology of Nylon-6 and Poly (ethylene-ran-propylene) Rubber Blends. *Macromolecules* **2004**, *37*, 2454−2459.
(23) Li, Y. J.; Shimizu, H. Conductive PVDF/PA6/CNTs Nanocomposites Fabricated by Dual Formation of Cocontinuous and Nanodispersion Structures. *Polymer* **2004**, *45*, 7381−7388.
(24) Wang, Y.; Zhang, Q.; Fu, Q. Compatibilization of Immiscible Poly (propylene)/Polystyrene Blends Using Clay. *Macromol. Rapid Commun.* **2003**, *24*, 231−235.
(25) Zou, H.; Zhang, Q.; Tan, H.; Wang, K.; Du, R. N.; Fu, Q. Clay Locked Phase Morphology in the PPS/PA66/Clay Blends during Compounding in an Internal Mixer. *Polymer* **2006**, *47*, 6−11.
(26) Chow, W. S.; Mohd Ishak, Z. A.; Karger-Kocsis, J.; Apostolov, A. A.; Ishiaku, U. S. Compatibilizing Effect of Maleated Polypropylene on the Mechanical Properties and Morphology of Injection Molded Polyamide 6/Polypropylene/Organoclay Nanocomposites. *Polymer* **2003**, *44*, 7427−7440.
(27) Wu, D. F.; Wu, L. F.; Zhang, M.; Zhou, W. D.; Zhang, Y. S. J. Morphology Evolution of Nanocomposites Based on Poly(phenylene sulfide)/Poly(butylene terephthalate) Blend. *J. Polym. Sci., Part B: Polym. Phys.* **2008**, *46*, 1265−1279.
(28) Liu, H.; Chen, F.; Liu, B.; Estep, G.; Zhang, J. Super Toughened Poly(lactic acid) Ternary Blends by Simultaneous Dynamic Vulcanization and Interfacial Compatibilization. *Macromolecules* **2010**, *43*, 6058−6066.
(29) Liu, H.; Song, W.; Chen, F.; Guo, L.; Zhang, J. Interaction of Microstructure and Interfacial Adhesion on Impact Performance of Polylactide (PLA) Ternary Blends. *Macromolecules* **2011**, *44*, 1513−1522.
(30) Fu, Y.; Zhang, J.; Liu, H.; Hiscox, W. C.; Gu, Y. Ionic Liquid-assisted Exfoliation of Graphite Oxide for Simultaneous Reduction and Functionalization to Graphenes with Improved Properties. *J. Mater. Chem. A* **2013**, *1*, 2663−2674.
(31) Fasolino, A.; Los, J.; Katsnelson, M. Intrinsic Ripples in Graphene. *Nat. Mater.* **2007**, *6*, 858−861.
(32) Dreyer, D. R.; Park, S.; Bielawski, C. W.; Ruoff, R. S. The Chemistry of Graphene Oxide. *Chem. Soc. Rev.* **2010**, *39*, 228−240.
(33) Singh, V.; Joung, D.; Zhai, L.; Das, S.; Khondaker, S. I.; Seal, S. Graphene Based Materials: Past, Present and Future. *Prog. Mater. Sci.* **2011**, *56*, 1178−1271.
(34) Filippone, G.; Dintcheva, N. T.; La Mantia, F.; Acierno, D. Using Organoclay to Promote Morphology Refinement and Co-continuity in High-Density Polyethylene/Polyamide 6 Blends-Effect of Filler Content and Polymer Matrix Composition. *Polymer* **2010**, *51*, 3956−3965.
(35) Hong, J. S.; Namkung, H.; Ahn, K. H.; Lee, S. J.; Kim, C. The Role of Organically Modified Layered Silicate in the Breakup and Coalescence of Droplets in PBT/PE Blends. *Polymer* **2006**, *47*, 3967−3975.
(36) Persenaire, O.; Raquez, J. M.; Bonnaud, L.; Dubois, P. Tailoring of Co-Continuous Polymer Blend Morphology: Joint Action of Nanoclays and Compatibilizers. *Macromol. Chem. Phys.* **2010**, *211*, 1433−1440.
(37) Fenouillot, F.; Cassagnau, P.; Majeste, J.-C. Uneven Distribution of Nanoparticles in Immiscible Fluids: Morphology Development in Polymer Blends. *Polymer* **2009**, *50*, 1333−1350.
(38) Wu, S. *Polymer Interface and Adhesion*, 1st ed.; Marcel Dekker, Inc.: New York, 1982.
(39) Xu, Z. H.; Zhang, Y. Q.; Wang, Z. G.; Sun, N.; Li, H. Enhancement of Electrical Conductivity by Changing Phase Morphology for Composites Consisting of Polylactide and Poly(ε-caprolactone) Filled with Acid-oxidized Multiwalled Carbon Nanotubes. *ACS Appl. Mater. Interfaces* **2011**, *3*, 4858−4864.
(40) Grossiord, N.; Loos, J.; Van Laake, L.; Maugey, M.; Zakri, C.; Koning, C. E.; Hart, A. J. High-Conductivity Polymer Nanocomposites Obtained by Tailoring the Characteristics of Carbon Nanotube Fillers. *Adv. Funct. Mater.* **2008**, *18*, 3226−3234.
(41) Fuhrer, M.; Nygård, J.; Shih, L.; Forero, M.; Yoon, Y.-G.; Choi, H. J.; Ihm, J.; Louie, S. G.; Zettl, A.; McEuen, P. L. Crossed Nanotube Junctions. *Science* **2000**, *288*, 494−497.
(42) He, F.; Lau, S.; Chan, H. L.; Fan, J. High Dielectric Permittivity and Low Percolation Threshold in Nanocomposites Based on Poly (vinylidene fluoride) and Exfoliated Graphite Nanoplates. *Adv. Mater.* **2009**, *21*, 710−715.